Available online at www.sciencedirect.com
SCIENCE DIRECT®
Journal of Solid State Chemistry 177 (2004) 690–695
JOURNAL OF SOLID STATE CHEMISTRY
http://elsevier.com/locate/jssc

Controlled synthesis of single-crystal $VO_x \cdot nH_2O$ nanoribbons via a hydrothermal reduction method

Lingfen Kong, Zhaoping Liu, Mingwang Shao, Qin Xie, Weichao Yu, and Yitai Qian*

Structure Research Laboratory and Department of Chemistry, University of Science and Technology of China, Hefei, Anhui 230026, People's Republic of China

Received 9 June 2003; received in revised form 7 August 2003; accepted 19 August 2003

Abstract

$VO_x \cdot nH_2O$ ($2.0 \leqslant x \leqslant 2.5$) nanoribbons have been synthesized by direct hydrothermal processing of the aqueous solution of NH_4VO_3 and polyethylene glycol 400 (PEG-400) at pH 3.5–5.5. Techniques of XRD, SEM, TEM, HRTEM, ED, and XPS have been used to characterize the structure, morphology, and composition of the nanoribbons. The $VO_x \cdot nH_2O$ nanoribbons are up to ~200 μm in length, 100–150 nm in width, 20–30 nm in thickness, and grow along the [010] direction. The ratios of V^{4+} to V^{5+} in the products can be readily controlled by carefully adjusting the periods of reaction time. PEG carries the roles of both transport and reducing agent. A coordination self-assembly mechanism was proposed to elucidate the formation of the $VO_x \cdot nH_2O$ nanoribbons.

Keywords: Vanadium oxides; PEG; Nanoribbons; Hydrothermal synthesis

1. Introduction

In recent years, vanadium oxides and their derivate compounds have attracted much attention due to their special physical and chemical properties and potential applications in areas such as catalysts [1], high-energy density lithium batteries [2,3], chemistry sensors [4], electrochemical and optical devices [5,6]. V_2O_5 is in layered structure in which VO_5 square pyramids (SPs) are connected by sharing corners and edges [7–9]. While part of V^{5+} cations are reduced to V^{4+} cations, VO_4 tetrahedra appear together with the typical VO_5 SPs. Therefore the structure of VO_x ($2.0 \leqslant x \leqslant 2.5$) consists of both VO_5 SPs and VO_4 tetrahedra. The SPs share edges to form zigzag chains in the [010] direction, and these chains are connected by corner-sharing SPs and tetrahedra [7]. Thus, the presence of changeable ratio of V^{4+}/V^{5+} contributes to the multitude of imaginable of already obtained structures, which allows for tailorable physical properties of as-synthesized products [6]. Recently, Various methods have been developed to synthesize vanadium oxides 1D nanostructures. For example, thin film of $V_2O_5 \cdot nH_2O$ xerogel consisting of ribbon-like nanoparticles have been synthesized by sol–gel process from different V^{5+} species [10–12]; $V_2O_5 \cdot nH_2O$ nanowires have been synthesized by hydrothermal reaction from NH_4VO_3 aqueous solution [13]; Vanadium oxide nanotubes (VO_x-NTs) could be obtained in the presence of organic molecules as structure-directing templates [14,15].

Herein, we report a high-yielding synthesis method of uniform $VO_x \cdot nH_2O$ nanoribbons by hydrothermal processing of the solution of NH_4VO_3 and polyethylene glycol 400 (PEG-400). The ratios of V^{4+} to V^{5+} in the products can be controlled by carefully adjusting reaction time. We carried series of experiments to investigate the formation mechanism of the nanoribbons.

2. Experimental section

In a typical procedure, analytically pure NH_4VO_3 (0.116 g, 1 mmol) and PEG-400 (0.4 g, 1 mmol) were dissolved into 50 mL distilled water. An appropriate amount of 0.1 M HNO_3 was added to the mixture solution to adjust pH in the range 3.5–5.5. Then the solution was put into a 60-mL autoclave with a Teflon

*Corresponding author. Fax: +865513607402.
E-mail addresses: lfkong@mail.ustc.edu.cn (L. Kong), ytqian@ustc.edu.cn (Y. Qian).

0022-4596/$ - see front matter © 2003 Elsevier Inc. All rights reserved.
doi:10.1016/j.jssc.2003.08.035

liner. The autoclave was maintained at 180°C for different periods of time and then cooled to room temperature naturally. Precipitate was collected and washed with deionized water and anhydrous alcohol for several times. The finial product was dried in vacuum at 60°C for 4 h.

The X-ray diffraction was carried out on a Rigaku (Japan) D/max-rA X-ray diffractionmeter equipped with graphite monochromatized Cu$K\alpha$ radiation ($\lambda = 1.54178$ Å). The scan rate 0.06°/s was applied to record the pattern in the 2θ rang of 5–65°. The SEM images were taken with a field emission scanning electron microscope (JEOL-6300F, 15 kV). The TEM images were performed with a Hitachi 800 transmission electron microscopy performed at 200 kV. The HRTEM images and the corresponding selected area electron diffraction patterns were taken on a JEOL 2010 high-resolution transmission electron microscope performed at 200 kV. The X-ray photoelectron spectra (XPS) were recorded on a VGESCALAB MKII X-ray photoelectron spectrometer with an exciting source Mg$K\alpha$ (1253.6 eV).

3. Results and discussion

Vanadium oxide phases with mixed valency, containing V^{5+} as well as V^{4+} cations, were usually obtained by hydrothermal processing of precursor and reductive organic molecules [14,15]. In the present study, PEG-400 was also served as reducing agent. The products appeared various colors: after hydrothermal processing for 8 h, the color of the product changed from yellow to pea green, which indicated that V^{5+} cations partially reduced to V^{4+} cations [11]; Further prolonging the reaction time, the color changed to deep-green. After 72 h, the color changed to blue, which makes clear that all V^{5+} cations had been reduced to V^{4+} cations. Color change of the samples suggested that percent of V^{4+} in total V of vanadium oxide increased with reaction time elongating.

Shown in Fig. 1 are the XRD patterns of the samples obtained by hydrothermal treatment for 4, 8, 24, 48, and 72 h, respectively. The XRD patterns shown in Fig. 1(a–d) are characteristic of (00l) reflections for layered vanadium oxide. These data are similar to reported XRD data in Refs. [7,16,17]. Furthermore, both PEG and other organic molecules had not been detected in these samples through FTIR analysis. Thus only water molecules were embedded between the layers [18,19]. Judged from XRD patterns and colors of the samples, the products can be identified to layered $V_2O_5 \cdot nH_2O$ phase (4 h) with a layer spacing of 1.10 nm, and layered $VO_x \cdot nH_2O$ phases (more than 8 h) with different layer spacings. Since the layer spacings of $V_2O_5 \cdot nH_2O$ vary with water contents, e.g.,

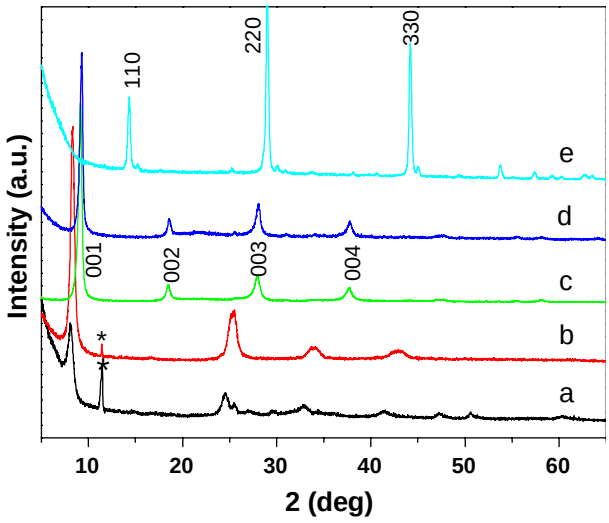

Fig. 1. XRD patterns of the samples synthesized at 180°C for different periods of reaction time. (a) 4 h; (b) 8 h; (c) 24 h; (d) 48 h; and (e) 72 h. *$(NH_4)_4V_6O_{17} \cdot 14H_2O$ phase (JCPDS 21-41).

1.15 nm for $n \sim 1.6$ and 0.87 nm for $n \sim 0.5$ [17], the n value of the sample (4 h) can be estimated to be between 0.5 and 1.6. As to the $VO_x \cdot nH_2O$ phase, the layer spacing is 1.06 nm (8 h), 0.97 nm (24 h), and 0.95 nm (48 h), respectively. On the other hand, XPS analyses (Fig. 2a–d) demonstrate that the ratio of V^{4+} to V^{5+} is $\sim 1/4$ (24 h) and $\sim 1/2.3$ (48 h). Namely, x values of $VO_x \cdot nH_2O$ phases obtained for 24 h and 48 h are 2.40 and 2.33, respectively. After 72 h, $V_2O_5 \cdot nH_2O$ was completely reduced to rutile-type structure VO_2 (JCPDS 42-876) (Fig. 1e). The results suggested that with reaction time elongating, the values of both x and n decreased.

SEM observations illuminate that the products consist entirely of very long ribbon-like nanostructures with lengths in the range of several tens to several hundreds of micrometers (Fig. 3a). The yield of the nanoribbons is greater than 95% by statistic. The twist and waving shapes of the ribbons are apparent. Fig. 3b shows that the nanoribbons are highly flexible. The nanoribbons have rectangle-like cross sections and relatively uniform widths of 100–150 nm and thicknesses of 20–30 nm along their entire length (see Fig. 3c and d).

Shown in Fig. 4 are HRTEM image and corresponding ED pattern of a single nanoribbon obtained by hydrothermal processing for 24 h. Evidently, The ribbon is single crystalline and free from dislocations. Its surface is clean without an amorphous layer. Although the percent of V^{4+} in total V get up to 20% based on the XPS analysis, The ED pattern (inset of Fig. 4) is yet in accord with orthorhombic V_2O_5 phase (JCPDS 41-1426). In the HRTEM image, the lattice spacing of the nanoribbon is 0.58 nm, corresponding to (200) diffraction spot of the ED pattern. The HRTEM image and the ED pattern demonstrate that the initial $V_2O_5 \cdot nH_2O$

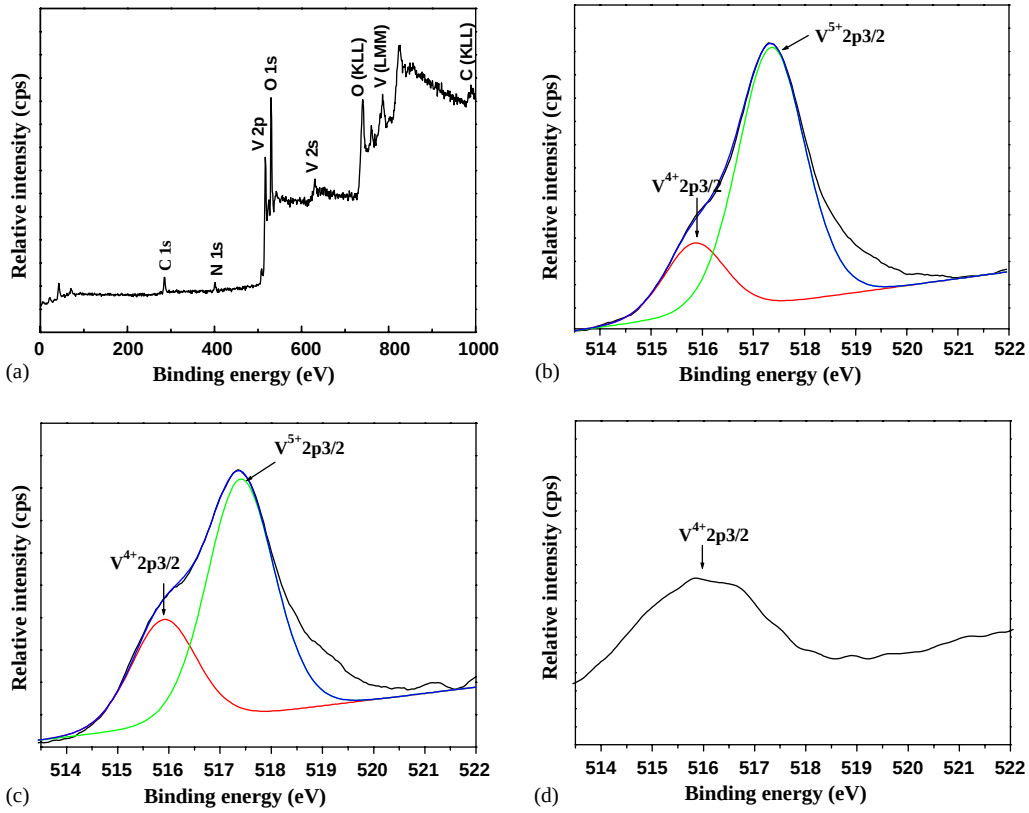

Fig. 2. (a) XPS survey spectrum of the product; The binding energy spectrum for V^{4+} $2p3/2$ and V^{5+} $2p3/2$ of the samples synthesized at 180°C for different periods of time (b) 24 h; (c) 48 h; and (d) 72 h. The two peaks at 515.9 and 517.4 eV are corresponding to the excitation of $V^{4+}2p3/2$ and $V^{5+}2p3/2$, respectively. The quantifications of XPS peaks give the molar ratio of V^{4+} to V^{5+} of the as-prepared samples obtained for 24 h as 1:4 and 48 h as 1:2.3, respectively. The XPS spectrum in Fig. 2(d) shows that V^{5+} cations were not presented in the sample obtained for 72 h.

nanoribbons grow along [010] direction enclosed with the {100} and {001} as side and top planes. It is worth noting that the $VO_x \cdot nH_2O$ nanoribbons were transformed from the reduction of $V_2O_5 \cdot nH_2O$ nanoribbons. This means that a certain amount of total VO_5 SPs had translated into VO_4 tetrahedra. VO_5 SPs as well as VO_4 tetrahedra were still connected by sharing corners or edges, and then the layered structure was maintained. The crystal structure of as-synthesized $VO_x \cdot nH_2O$ was similar to that of $V_2O_5 \cdot nH_2O$. Therefore, it is not surprising that the lattice spacing and ED pattern of $VO_x \cdot nH_2O$ are consistent with those of V_2O_5 phase.

To gain a better understanding of the mechanism of the nanoribbon growth, we have studied the influence of reaction time on the products by SEM, TEM, and XRD. After hydrothermal treatment at 180°C for 2 h, the product was a yellow mixture of particles and floccules: the major product was yellow particles with regular polyhedron in morphologies and tens of micrometers in sizes, while a small quantity of the product was yellow floccules. Because of their distinct morphologies and sizes of the two products, they could be easily separated from each other. The XRD patterns indicated that the yellow particles were $(NH_4)_4V_6O_{17} \cdot 14H_2O$ crystals and the floccules were $V_2O_5 \cdot nH_2O$, respectively. Fig. 5a shows SEM image of the floccules mainly consisting of short fibrillar nanostructures. The nanofibers (<5 μm in length) seemed to emanate from one center and grow in all directions thus shaping 3D star-like nanoflower patterns. Closer inspection revealed that the geometrical shapes of the fibrillar nanostructures appeared to be short and wide ribbons (Fig. 5b). Subsequently, with prolonging reaction time, the yield of floccules increased sharply, while the percent of $(NH_4)_4V_6O_{17} \cdot 14H_2O$ crystals decreased, and the crystals disappeared after ~12 h. As the reaction time was elongated to 8 h (Fig. 5c), the nanoflowers consisted of much more, thinner and longer ribbons, and therefore the radial growth pattern of nanoribbons was clearly discernable. This suggests that the second and side nucleation of the nanoribbons occurred at the tied region of short and wide incipient ribbons (shown in Fig. 5b), and they all grew along [010] direction. After 16 h (Fig. 5d), the nanoflowers disappeared, and separate ribbons with lengths of ~150 μm and widths of ~120 nm could be observed. ED pattern (inset of Fig. 5d) indicates the nanoribbons were single crystalline. Further elongating reaction time, the lengths of

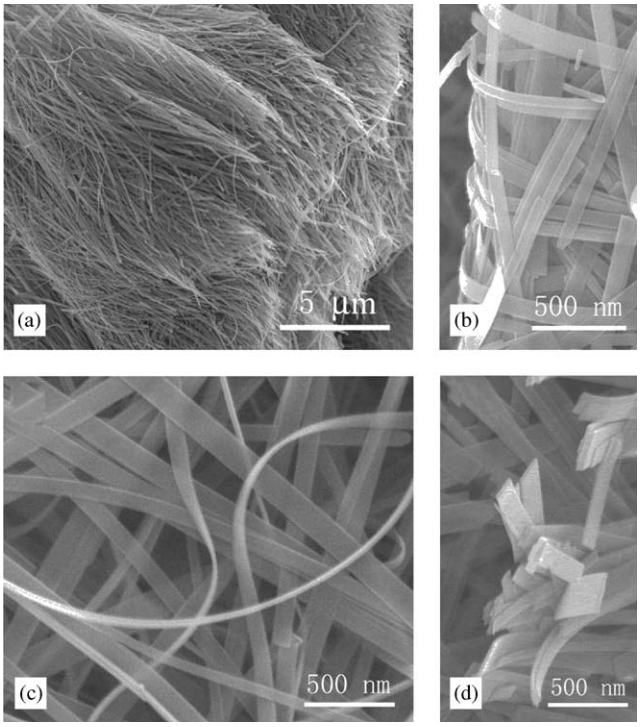

Fig. 3. SEM images of the $VO_x \cdot nH_2O$ samples synthesized at 180°C for 24 h. (a) Shows the nanoribbons with high purity, high yield, and ultra-long and uniform morphology; (b) and (c) display the characteristic features of $VO_x \cdot nH_2O$ nanoribbons; (d) shows rectangle-like cross-sections of the nanoribbons.

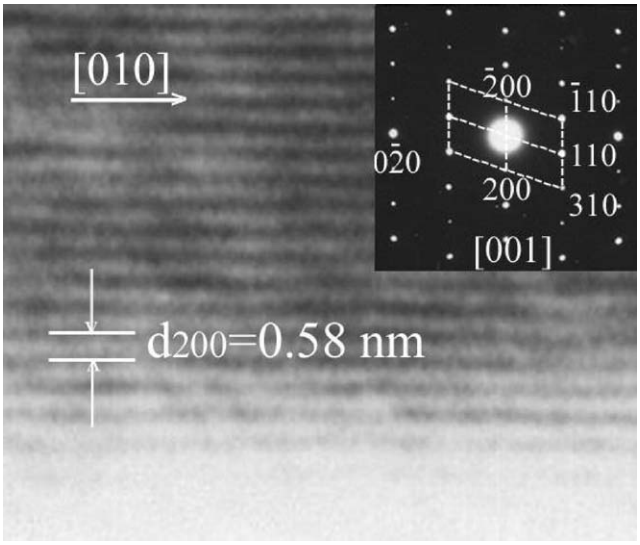

Fig. 4. HRTEM image recorded near the edge of $VO_x \cdot nH_2O$ nanoribbon along the direction perpendicular to the wide surface of the nanoribbon. The white arrow shows its growth direction. The inset shows the corresponding SAED pattern along the [001] axis.

nanoribbons did not increase strikingly, while the ratio of V^{4+} to V^{5+} increased slowly until all the V^{5+} cations were finally reduced to V^{4+} cations.

As for the NH_4VO_3-HNO_3 hydrothermal reaction system, the previous study suggested that vanadium

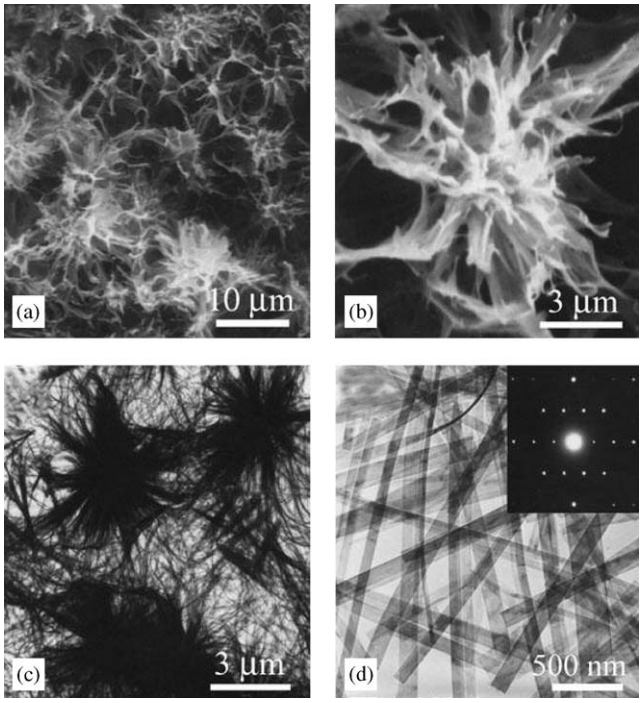

Fig. 5. SEM and TEM images of the products that were synthesized by hydrothermal reaction at 180°C for (a) and (b) 2 h, (c) 8 h, and (d) 24 h, respectively.

oxide 1D nanostructures could be produced only in a narrow range of pH values (2–3) [13]. Practically, we found that only $(NH_4)_4V_6O_{17} \cdot 14H_2O$ microcrystals could be observed out of this range of pH values. Nevertheless, when PEG-400 was supplementally put into the above reaction solution containing the produced $(NH_4)_4V_6O_{17} \cdot 14H_2O$ crystals, and then the mixture was maintained at 180°C for 10 h, $VO_x \cdot nH_2O$ nanoribbons would be obtained again. The above results suggested that PEG was critical to the formation of $VO_x \cdot nH_2O$ nanoribbons at a higher pH value (>3). Some polymers (such as PVP, PEO, and PEG), which are a multidentate ligands with poly functional groups, have served as bridging ligands to form multinuclear complexes [20–22]. From above results and the phase diagram of V (V) in aqueous solutions [23], we assumed that a coordination complex PEG_x-$V_{10}O_{27}(OH)^{5-}$ created under the hydrothermal conditions. PEG molecule chain may afford its O atoms to coordinate with V^{5+} of the polyvanadate ions. Therefore, a coordination self-assembly mechanism was used to elucidate the formation of $V_2O_5 \cdot nH_2O$ nanoribbons.

Supported by the above analyses, the whole reaction process may be represented by the following equations:

$$10VO_3^- + 5H^+ \rightarrow V_{10}O_{27}(OH)^{5-} + 2H_2O, \quad (1)$$

$$3V_{10}O_{27}(OH)^{5-} + 20NH_4^+ + 15H_2O \rightleftharpoons 5(NH_4)_4V_6O_{17} \cdot 14H_2O + 5H^+, \quad (2)$$

Table 1
The real precursors in 20 mM NH_4VO_3 aqueous solution at different pH values and the corresponding final products obtained in the presence of PEG-400 after hydrothermal treatment at 180°C for 48 h. The precursors were concluded according to the phase diagram of V (V) species in Ref. [17]. The phases of the products were determined by XRD analysis

pH	<1	1–3	3–3.5	3.5–5.5	5.5–5.9	5.9–9
Precursors	VO_2^+	V_2O_5	$V_{10}O_{26}(OH)_2^{4-}$	$V_{10}O_{27}(OH)^{5-}$	$V_{10}O_{28}^{6-}$	$V_3O_9^{3-}$
Products	—	$VO_2 + VO_x \cdot nH_2O$	$VO_x \cdot nH_2O$	$VO_x \cdot nH_2O$	$VO_x \cdot nH_2O$	$(NH_4)_2V_4O_9 + VO_x \cdot nH_2O$[a,b]

Notes: –, no product was found.
[a] With increasing of pH, the yield of $(NH_4)_2V_4O_9$ increased, and only $(NH_4)_2V_4O_9$ could be obtained when pH is more than 8.
[b] JCPDS 23–791.

$$V_{10}O_{27}(OH)^{5-} + PEG_x \rightleftharpoons PEG_x\text{-}V_{10}O_{27}(OH)^{5-}, \quad (3)$$

$$PEG_x\text{-}V_{10}O_{27}(OH)^{5-} + 5H^+ \rightarrow 5V_2O_5 \cdot nH_2O + PEG_x + 3H_2O, \quad (4)$$

$$V_2O_5 \cdot nH_2O \xrightarrow{PEG} VO_x \cdot nH_2O \text{ or } VO_2. \quad (5)$$

The polyvanadate ion, $V_{10}O_{27}(OH)^{5-}$, was transformed from VO_3^- (20 mM, pH 3.5–5.5). Substantially, $(NH_4)_4V_6O_{17} \cdot 14H_2O$ crystals were first created by polycondensation of the polyvanadate ions when the temperature was increased. When PEG was introduced into this solution, the forming complex PEG_x-$V_{10}O_{27}(OH)^{5-}$ brought on the dissolution of the formed $(NH_4)_4V_6O_{17} \cdot 14H_2O$ based on Eq. (2) under present hydrothermal conditions. Then this complex would gradually condense into solid phase $V_2O_5 \cdot nH_2O$, and seeds (nanoflowers) appeared in the heating solution through a homogenous nucleation. Then the nanoflowers grew longer and shaped into separate nanoribbons. These nanoribbons could continuously grow along with [010] direction until all $V_{10}O_{27}(OH)^{5-}$ had been completely consumed. Furthermore, in a separate experiment, when another alcohol (for example, ethanol, glycol, and glycerol) was used instead of PEG, ribbon-like vanadium oxide could also be obtained, but they were very short and not uniform. This means that a complex of polyvanadate ions and alcohol can also form based on a reaction similar to Eq. (3) under the hydrothermal conditions. However, PEG may be more suitable for the formation of long and uniform ribbons due to its chain-like structure. We also found that the length of PEG molecule chain had little influence on the shape and size of the product.

As we know, vanadium in its higher oxidation state gives various isopolyvanadates at different pH values in aqueous solution [23], so we have made a set of experiments to investigate the influence of pH value on the final product. Table 1 shows the real precursors in 20 mM NH_4VO_3 aqueous solution at different pH values and the final products obtained in the presence of PEG-400 after hydrothermal treatment at 180°C for 48 h. $VO_x \cdot nH_2O$ could be always obtained in a relatively wide range of pH values (pH 1–8) although the polyoxovanadate precursors were different in such pH range. These results further suggested that the complex of polyoxovanadate and PEG was created from any polyoxovanadate. Compared to previous reports [14,15], in the presence of PEG, the suitable pH values for the formation of $VO_x \cdot nH_2O$ nanoribbons are extended into a very wide range.

On the other hand, the formation of $VO_x \cdot nH_2O$ nanoribbons containing various amounts of V^{4+} would attribute to the reduction of V^{5+} by PEG according to the period of reaction time, and VO_2 nanoribbons would be finally produced after 72 h. Because of the very slow rate for the reduction of V^{5+}, and the similarity in 3D network structures between $V_2O_5 \cdot nH_2O$ and $VO_x \cdot nH_2O$, the ribbon-like morphology of the product could be maintained all the time. This suggests that $VO_x \cdot nH_2O$ nanoribbons with various ratio of V^{4+} to V^{5+} can be readily obtained by carefully controlling the reaction time.

4. Conclusion

In summary, we have successfully synthesized $VO_x \cdot nH_2O$ nanoribbons which are lengths of up to several hundreds of micrometers with rectangle typically widths of 100–150 nm and thicknesses of 20–30 nm. The formation of nanoribbons greatly relies on the presence of PEG.A coordination self-assembly process was used to explain the formation mechanism of the $VO_x \cdot nH_2O$ nanoribbons. More studies about this complex PEG_x-$V_{10}O_{27}(OH)^{5-}$ are still in progress. Moreover, by carefully adjusting period of the reaction time, various amounts of V^{4+} accounting for total V in the finial product can be readily controlled. It promises the tailorable physical properties in nanodevices.

Acknowledgments

This work was supported by National Natural Science Foundation of China and the 973 Project of China.

References

[1] L.J. Durand-Keklikian, Electroanal. Chem. 527 (2002) 112.
[2] P.P. Prosini, Y.Y. Xia, T. Fujieda, R. Vellone, M. Shikano, T. Sakai, Electrochimica Acta 46 (2001) 2623.
[3] P.P. Prosini, T. Fujieda, S. Passerini, T. Sakai, Electrochem. Commun. 2 (2000) 4.
[4] P. Liu, S.H. Lee, H.M. Cheong, C.E. Tracy, J.R. Pitts, R.D. Smith, J. Electrochem. Soc. 149 (2002) H76.
[5] J. Muster, G.Y. Kini, V. Krstić, J.G. Park, Y.W. Park, S. Roth, M. Burghard, Adv. Mater. 12 (6) (2000) 420.
[6] J.-F. Xu, R. Czerw, S. Webster, D.L. Carroll, Appl. Phys. Lett. 81 (9) (2002) 1717.
[7] T. Chirayil, P.Y. Zavalij, M.S. Whittingham, Chem. Mater. 10 (1998) 2629.
[8] J. Livage, Chem. Mater. 3 (1991) 578.
[9] Y. Kanke, K. Kato, E. Takayama-Muromachi, M. Isobe, Acta Crystallogr. C 46 (1990) 536.
[10] J.H.L. Watson, W. Heller, W. Wojtowicz, Science 109 (1949) 275.
[11] J. Livage, Chem. Mater. 3 (1991) 578.
[12] J.K. Bailey, G.A. Pozarnsky, M.L. Mecartney, J. Mater. Res. 7 (9) (1992) 2530.
[13] D.Y. Pan, S.Y. Zhang, Y.Q. Chen, J.G. Hou, J. Mater. Res. 17 (8) (2002) 1981.
[14] F. Krumeich, H.J. Muhr, M. Niederberger, F. Bieri, B. Schnyder, R. Nesper, J. Am. Chem. Soc. 121 (1999) 8324.
[15] X. Chen, X.M. Sun, Y.D. Li, Inorg. Chem. 41 (17) (2002) 4524.
[16] V. Petkov, P.N. Trikalitis, E.S. Bozin, S.J.L. Billinge, T. Vogt, M.G. Kanatzidis, J. Am. Chem. Soc. 124 (2002) 10157.
[17] T. Yao, Y. Oka, N. Yamamoto, Mater. Res. Bull. 27 (1992) 669.
[18] H.P. Oliviera, C.F.O. Graeff, J.M. Rosolen, Mater. Res. Bull. 34 (1999) 1891.
[19] G.J.-F. Demets, F.J. Anaissi, H.E. Toma, M.B.A. Fontes, Mater. Res. Bull. 37 (2002) 683.
[20] Y. Deng, G.D. Wei, C.W. Nan, Chem. Phys. Lett. 368 (2003) 639.
[21] R.D. Rogers, J.H. Zhang, C.B. Bauer, J. Alloys Compd. 249 (1997) 41.
[22] M.M.S. Puga, L.D. Carlos, T.M.A. Abrantes, L. Alcacer, Chem. Mater. 7 (1995) 2316.
[23] J. Livage, Coord. Chem. Rev. 178–180 (1998) 999.